Digital Implementation of Deadbeat-Direct Torque and Flux Control for Permanent Magnet Synchronous Machines in the *M-T* Reference Frame

Yuefei Zuo, *Member, IEEE*, Jie Mei, *Student Member, IEEE*, Chaoqiang Jiang, *Member, IEEE*, and Christopher H. T. Lee, *Senior Member, IEEE*

***Abstract*- In the traditional deadbeat-direct torque and flux control in the *M-T* reference frame (DB-DTFC-MT) scheme, the stator flux is calculated with the current model, and one-step delay in the digital system is neglected, which results in poor robustness to parameter variations and a serious oscillation in both the stator flux and torque, especially in the low-speed range. In this paper, the digital implementation of DB-DTFC-MT is studied. Firstly, the DB-DTFC-MT scheme considering the one-step delay in the digital system is deduced. Secondly, digital stator flux observer and current observer are developed to predict the stator flux and current in the next sampling instant. By using the predicted stator flux and torque, the oscillation caused by the one-step delay is eliminated and real deadbeat control is realized. Moreover, the robustness of the system to parameter variations is qualitatively evaluated. Though the system shows some sensitivity to the permanent magnet flux, it has strong robustness to the stator resistance and inductances, especially the *d*-axis inductance. Hence, a larger estimated *d*-axis inductance can be used in the system for reducing the pulsation in the *d*-axis current when tracking sinusoidal torque. All the proposed control designs are validated on a real-time control platform based on dSPACE DS1103.**

***Index Terms*—Current observer, deadbeat, direct torque and flux control (DTFC), one-step delay, stator flux observer.[1]**

I. INTRODUCTION

IN the field-oriented control (FOC) system, the *d*- and *q*-axis stator current vector components are selected as the control state variables [1], thus FOC is also called current vector control (CVC). Since the stator current vector is treated as the manipulated input, FOC puts the control of torque and flux in an open-loop control state [2]. Therefore, the torque generation is more challenging when the magnetizing inductance is saturated and the available voltage and/or current is limited [3], [4].

Direct torque control (DTC) selects estimated torque and stator flux magnitude as two control state variables and applies a closed-loop feedback control structure to regulate these states. Therefore, to be precise, DTC should be called direct torque and flux control (DTFC) since both torque and stator flux are simultaneously controlled [1]. The basic DTFC controls stator flux and torque by a hysteresis comparator and a switching table, which is a suitable methodology that requires little knowledge of machine physics. Consequently, compared with FOC, the basic DTFC has many advantages, such as eliminating coordinate transformation, less parameter dependence, and faster dynamic response [5]. Nevertheless, such bang/bang control methods are known to produce a variable switching frequency, which makes it very challenging to integrate signal injection techniques for low-speed self-sensing control. In order to achieve reduced ripple and constant switching frequency, numerous improved DTFC schemes utilizing space vector modulation (DTFC-SVM) are proposed [6].

In the existing DTFC-SVM methods, the DTFC scheme in the *d-q* reference frame is attractive because it is easy to integrate with the self-sensing control method based on high-frequency injection. However, in the continuous-time domain, it is difficult to decouple the manipulated inputs (*d-q* voltage components) from their effects on the airgap torque and stator flux. Therefore, the deadbeat direct torque and flux controller in the *d-q* reference frame (DB-DTFC-DQ) is proposed for induction machine drives [7] and interior PMSM (IPMSM) drives [8]. The DB-DTFC-DQ scheme shows better robustness to motor parameter variations [9] and superior flux weakening performance [10] than the CVC scheme based on the proportional-integral (PI) control. Nevertheless, the DB-DTFC-DQ scheme is time-consuming due to the nature of cross-coupling between the torque and the stator flux.

Due to the decoupling properties between the stator flux and torque, the DTFC scheme in the *M-T* reference frame (DTFC-MT) was developed to regulate the torque and stator flux independently [11]. Since the linear relationship between the control states and the manipulated inputs, the stator flux and torque can be regulated with two simple linear PI controllers [12], [13]. In [14], a deadbeat controller based on duty cycle

Manuscript received June 30, 2020; revised August 6, 2020; accepted September 15, 2020. This work was supported in part by the Start-Up Grant from Nanyang Technological University under Grant 04INS000574C140, and in part by the Natural Science Foundation of China under Grant 51807080. Recommended for publication by Associate Editor J. Hur. *(Corresponding author: Christopher H. T. Lee.)*

Y. Zuo is with the School of Electrical and Information Engineering, Jiangsu University, Zhenjiang 212013, China (e-mail: zuoyuefei@ujs.edu.cn)

J. Mei is with the Research Laboratory of Electronics, Massachusetts Institute of Technology, Cambridge, MA 02139, USA (e-mail: jiemei@mit.edu)

C. Jiang is with the Department of Electrical Engineering, University of Cambridge, Cambridge CB3 0FA, UK (e-mail: cj426@cam.ac.uk)

C. H. T. Lee is with the School of Electrical and Electronic Engineering, Nanyang Technological University, Singapore 639798, Singapore (e-mail: chtlee@ntu.edu.sg).

Color versions of one or more of the figures in this paper are available online at http://ieeexplore.ieee.org.

operation is proposed to improve the dynamic performance of the DTFC-MT system. However, big noise exists in the system since the one-step delay in the digital system is not considered. In [15], deadbeat DTFC-MT (DB-DTFC-MT) based on SVPWM is proposed. However, the one-step delay in the digital system is not considered and the current model is used to calculate the stator flux, resulting in poor robustness to parameter variations and serious oscillation in both the stator flux and torque, especially in the low-speed range.

In [16] and [17], closed-loop stator flux observer which combines the voltage model and the current model is proposed to estimate the rotor position. The closed-loop flux observer shows better robustness to parameter variations than the current model in the high-speed range and higher accuracy than the voltage model in the low-speed range [18], thus it can be used to realize wide-speed sensorless control [19]. In [20], a stator flux observer with phase self-tuning is proposed to improve the robustness of the sensorless control system to parameter variations. Since no high dynamic performance is required, the one-step delay in digital system is not considered.

In [21] and [22], the one-step delay in the digital system is considered in designing the DB-DTFC-DQ controller for induction machines. The stator flux observer and current observer are developed to predict the stator flux and torque. Similar observers are also used for PMSM drives [8], [9], [23]. Nevertheless, the design process of the DB-DTFC controller considering the one-step delay is not deduced in all these works. Moreover, the observer shown in this works cannot be directly used in the DB-DTFC-MT system.

In this paper, the digital implementation of DB-DTFC in the *M-T* reference frame is studied. Firstly, the DB-DTFC-MT scheme considering the one-step delay in the digital system is deduced. Secondly, digital stator flux observer and current observer are developed to predict the stator flux and current in the next sampling instant. By using the predicted stator flux and torque, the oscillation caused by the one-step delay is eliminated and real deadbeat control is realized. Due to the linearization of the state equations in the *M-T* reference frame, the theoretical analysis the effect of the motor parameter variations becomes possible. Therefore, the robustness of the system to parameter variations is qualitatively evaluated. The paper is organized as follows. In Section II, the principle of the DB-DTFC in the *M-T* reference frame is clarified. In Section III, the digital implementation of DB-DTFC in the *M-T* reference frame is described in detail. In Section IV, the robustness of the system to parameter variations is discussed. Simulation results are presented and analyzed in Section V and conclusions are drawn in Section VI.

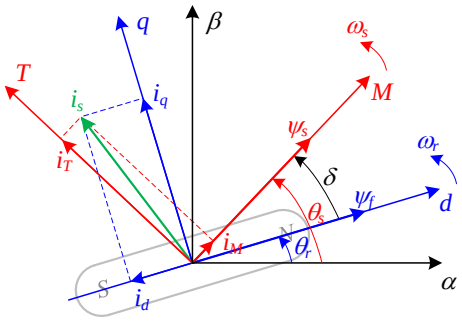

Fig. 1. Vector diagram of PMSM and coordinate axes.

II. Principle of DB-DTFC in the *M-T* Reference Frame

Fig. 1. shows the vector diagram and coordinate axes under steady-state operating conditions. The *α–β* reference frame is a stationary reference frame, whereas the *d–q* reference frame is a rotating frame synchronized with the rotor. The *M–T* reference frame is a rotating reference frame synchronized with the stator flux-linkage vector (ψ_s). The angles θ_r and θ_s indicate the positions of the rotor and the stator flux linkage vector, and ω_s and ω_r are the angular velocity of stator flux and rotor flux, respectively. δ and γ are the torque angle and the current angle, respectively.

The mathematical equations of PMSM in the *M-T* reference frame are as follows:

$$\begin{cases} u_M = R_s i_M + \dfrac{d\psi_M}{dt} - \omega_s \psi_T = R_s i_M + \dfrac{d|\psi_s|}{dt} \\ u_T = R_s i_T + \dfrac{d\psi_T}{dt} + \omega_s \psi_M = R_s i_T + \left(\omega_r + \dfrac{d\delta}{dt}\right)|\psi_s| \end{cases} \tag{1}$$

$$T_e = \frac{3p_n|\psi_s|}{4L_d L_q}\left[2L_q\psi_f \sin\delta + \left(L_d - L_q\right)|\psi_s|\sin 2\delta\right] \tag{2}$$

where ψ_M and ψ_T, i_M and i_T, u_M and u_T represent the stator flux linkages, armature currents, and armature voltages in the *M-T* reference frame, ψ_M equals the magnitude of the stator flux linkages, i.e., $\psi_M=|\psi_s|$, $\psi_T=0$, R_s is the armature resistance, L_d and L_q are inductances in the *d-q* reference frame, and p_n denotes the number of pole pairs.

The derivative of the torque can be expressed as

$$\frac{dT_e}{dt} = A|\psi_s|\frac{d\delta}{dt} + B\frac{d|\psi_s|}{dt} \tag{3}$$

where

$$A = \frac{3p_n}{2L_d L_q}\left[L_q\psi_f \cos\delta + \left(L_d - L_q\right)|\psi_s|\cos 2\delta\right]$$

$$B = \frac{3p_n}{2L_d L_q}\left[L_q\psi_f \sin\delta + \left(L_d - L_q\right)|\psi_s|\sin 2\delta\right]$$

Generally, the second term on the right of (3) is neglected since it is much smaller than the first. Thus (3) is simplified as

$$\frac{dT_e}{dt} = A|\psi_s|\frac{d\delta}{dt} = A(u_T - R_s i_T - \omega_r|\psi_s|) \tag{4}$$

According to (1) and (4), the state equation of the stator flux and the torque can be discretized as

$$\begin{cases} |\psi_s(k+1)| = |\psi_s(k)| + T_s\left[u_M(k) - R_s i_M(k)\right] \\ T_e(k+1) = T_e(k) + A(k)T_s\left[u_T(k) - R_s i_T(k) - \omega_r\psi_s(k)\right] \end{cases} \tag{5}$$

where T_s is the sampling time.

III. DIGITAL IMPLEMENTATION OF DB-DTFC-MT

A. One-step Delay in Digital System

When forming a deadbeat control model, it is often assumed that the sampling and computation take zero time. Consequently, the manipulated output is applied at the sampling instant, and no lag is present. In real digital system, however, there is limited amount of delay due to the calculation time of sampling, estimation and control, thus the manipulated input is updated with time delay. To avoid the interrupt change of the duty cycle, the manipulated input is usually updated at the end of the PWM cycle, which means one step delay.

As seen in Fig. 2, the states sampled at the sampling instant k are used to calculate the manipulated input. Suppose no error exists between the manipulated input and the sampled voltage, there is $u_{MT}(k)=u^*_{MT}(k-1)$, then the stator flux at the end of PWM cycle k can be estimated as

$$\begin{cases} \left|\psi_s\left(k+1|k\right)\right| = \left|\psi_s(k)\right| + T_s\left[u^*_M(k-1) - R_s i_M(k)\right] \\ T_e\left(k+1|k\right) = T_e(k) + A(k)T_s \\ \qquad \left[u^*_T(k-1) - R_s i_T(k) - \omega_r\left|\psi_s(k)\right|\right] \end{cases} \tag{6}$$

It shows that the stator flux at the end of PWM cycle k is decided by the manipulated input calculated in PWM cycle k–1. Consequently, the stator flux and the torque at the end of PWM cycle k+1 can be estimated as

$$\begin{cases} \left|\psi_s\left(k+2|k+1\right)\right| = \left|\psi_s(k+1)\right| + T_s\left[u^*_M(k) - R_s i_M(k+1)\right] \\ T_e\left(k+2|k+1\right) = T_e(k+1) + T_s A(k+1) \\ \qquad \left[u^*_T(k) - R_s i_T(k+1) - \omega_r\left|\psi_s(k+1)\right|\right] \end{cases} \tag{7}$$

In order to realize the deadbeat control of stator flux, the estimated stator flux and torque are forced to follow the stator flux reference $|\psi_s^*(k)|$ and $T_e^*(k)$, then the manipulated input at the end of PWM cycle k can be calculated by (8)

$$\begin{cases} u^*_M(k) = \dfrac{\left|\psi^*_s(k)\right| - \left|\psi_s(k+1)\right|}{T_s} + R_s i_M(k+1) \\ u^*_T(k) = R_s i_T(k+1) + \omega_r\left|\psi_s(k+1)\right| + \dfrac{T^*_e(k) - T_e(k+1)}{A(k+1)T_s} \end{cases} \tag{8}$$

It shows that the state variables at the sampling instant k+1 are needed to realize the deadbeat control. However, these variables are unknown at the sampling instant k and thus have to be substituted with their predicted values. In this case, the manipulated inputs are deduced as

$$\begin{cases} u^*_M(k) = \dfrac{\left|\psi^*_s(k)\right| - \left|\psi_s\left(k+1|k\right)\right|}{T_s} + R_s i_M\left(k+1|k\right) \\ u^*_T(k) = R_s i_T\left(k+1|k\right) + \omega_r\left|\psi_s\left(k+1|k\right)\right| + \\ \qquad \dfrac{T^*_e(k) - T_e\left(k+1|k\right)}{A\left(k+1|k\right)T_s} \end{cases} \tag{9}$$

According to (9), the block diagram of the deadbeat controller for the stator flux and torque is shown in Fig. 3.

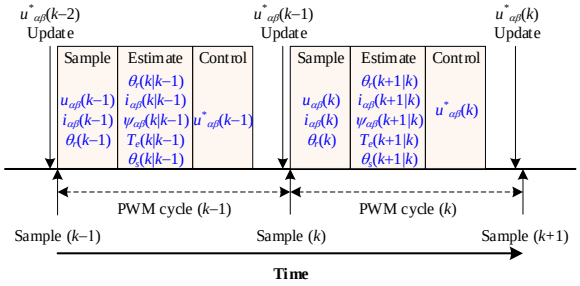

Fig. 2. Sequence and timing of events between sample instants.

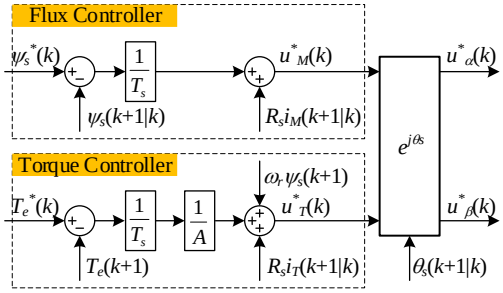

Fig. 3. Block diagram of the deadbeat controller for the stator flux and torque.

In DTFC system, the torque and stator flux magnitude are selected as the two control state variables. Observers are used to estimate these two variables since it is expensive or hard to measure them directly. In a digital system, a properly formed observer estimates values at the next sample instant based on the present values. This property is very important for a deadbeat control system.

B. The Stator Current Observer

Generally, the current observer is constructed in the d-q reference frame due to constant machine parameters. The voltage equation in the d-q reference frame can be written as follows using d-q complex vector notation:

$$\begin{aligned} \boldsymbol{u}_{dq} &= (R_s + j\omega_r L_{dq})\boldsymbol{i}_{dq} + L_{dq}\frac{d\boldsymbol{i}_{dq}}{dt}\boldsymbol{i}_{dq} + j\omega_r\psi_f \\ &= (\hat{R}_s + j\hat{\omega}_r\hat{L}_{dq})\boldsymbol{i}_{dq} + \hat{L}_{dq}\frac{d\boldsymbol{i}_{dq}}{dt} + j\hat{\omega}_r\hat{\psi}_f - \tilde{L}_{dq}\frac{d\boldsymbol{i}_{dq}}{dt} \\ &\quad -(\tilde{R}_s + j\tilde{\omega}_r L_{dq} + j\hat{\omega}_r\tilde{L}_{dq})\boldsymbol{i}_{dq} - j(\tilde{\omega}_r\psi_f + \hat{\omega}_r\tilde{\psi}_f) \\ &= (\hat{R}_s + j\hat{\omega}_r\hat{L}_{dq})\boldsymbol{i}_{dq} + \hat{L}_{dq}\frac{d\boldsymbol{i}_{dq}}{dt} + j\hat{\omega}_r\hat{\psi}_f - \Delta\boldsymbol{u}_{dq} \end{aligned} \tag{10}$$

$$\begin{aligned} \Delta\boldsymbol{u}_{dq} = (\tilde{R}_s + j\tilde{\omega}_r L_{dq} + j\hat{\omega}_r\tilde{L}_{dq})\boldsymbol{i}_{dq} + \tilde{L}_{dq}\,d\boldsymbol{i}_{dq}/dt + \\ j(\tilde{\omega}_r\psi_f + \hat{\omega}_r\tilde{\psi}_f) \end{aligned} \tag{11}$$

where $\boldsymbol{u}_{dq}$, $\Delta\boldsymbol{u}_{dq}$ and $\boldsymbol{i}_{dq}$ are the armature voltages, disturbance voltages and the armature currents in the d-q reference frame, $\hat{R}_s$, $\hat{L}_{dq}$, $\hat{\omega}_r$, and $\hat{\psi}_f$ are the estimated value of the stator resistance, d-q inductances, rotor speed, and the permanent magnet flux. $\tilde{R}_s = \hat{R}_s - R_s$ is the estimation error of the stator resistance. Similarly, $\tilde{L}_{dq}$, $\tilde{\omega}_r$, and $\tilde{\psi}_f$ are the estimation error of the d-q inductances, rotor speed, and the permanent magnet flux. These mismatches give rise to the disturbance voltages.

According to (10), the state equation of current in the d-q

reference frame can be written as

$$\frac{d\boldsymbol{i}_{dq}}{dt}=-\left(\frac{\hat{R}_s}{\hat{L}_{dq}}+j\hat{\omega}_r\right)\boldsymbol{i}_{dq}+\frac{1}{\hat{L}_{dq}}\left(\boldsymbol{u}_{dq}+\Delta\boldsymbol{u}_{dq}-j\hat{\omega}_r\hat{\psi}_f\right) \tag{12}$$

The observer constructed for the system expressed by (12) can be written in the form of

$$\begin{cases}\tilde{\boldsymbol{i}}_{dq}=\hat{\boldsymbol{i}}_{dq}-\boldsymbol{i}_{dq}\\ \dfrac{d\hat{\boldsymbol{i}}_{dq}}{dt}=-\left(\dfrac{\hat{R}_s}{\hat{L}_{dq}}+j\hat{\omega}_r\right)\boldsymbol{i}_{dq}+\dfrac{1}{\hat{L}_{dq}}\left(\begin{matrix}\boldsymbol{u}_{dq}+\Delta\hat{\boldsymbol{u}}_{dq}-\\ j\hat{\omega}_r\hat{\psi}_f-k_p\tilde{\boldsymbol{i}}_{dq}\end{matrix}\right)\\ \dfrac{d\Delta\hat{\boldsymbol{u}}_{dq}}{dt}=-k_i\tilde{\boldsymbol{i}}_{dq}\end{cases} \tag{13}$$

where $\tilde{\boldsymbol{i}}_{dq}$ and $\hat{\boldsymbol{i}}_{dq}$ are the observation error and the estimated stator current, respectively, k_p and k_i are the observer gains.

The estimated stator current can be obtained as

$$\hat{\boldsymbol{i}}_{dq}=\boldsymbol{i}_{dq}+\frac{\hat{L}_{dq}s}{\hat{L}_{dq}s^2+k_ps+k_i}\Delta\boldsymbol{u}_{dq} \tag{14}$$

The gains k_p and k_i can be set by pole placement, i.e., $k_p=2\hat{L}_{dq}\omega_{oi}$, $k_i=\hat{L}_{dq}\omega_{oi}^2$, where ω_{oi} is the undamped natural frequency of the current observer. It can be seen from (14) that the current observer acts as a state filter when neglecting the disturbance voltages. Stronger robustness to the disturbance voltages and better tracking performance can be obtained by using larger ω_{oi}, which, however, leads to poorer suppression of measurement noise [28], [29]. Therefore, ω_{oi} should be tuned to balance these performances. In this paper, it is set as 300Hz.

The block diagram of the current observer in discrete-time domain is shown in Fig. 4. It should be noted that $\hat{\boldsymbol{i}}_d$ is the estimation of $\boldsymbol{i}_{dq}(k)$ instead of $\boldsymbol{i}_{dq}(k+1)$, thus the predicted current $\boldsymbol{i}_{dq}(k+1|k)$ should be obtained from the left of the unit delay block. Since the current observer is developed in the *d-q* reference frame, inverse Park transformation is needed to obtain the predicted current in the α-β reference frame. Another key point is that the rotor angle used in the Park transformation should also be predicted.

C. The Stator Flux Observer

The flux-linkage is usually estimated by a mixed observer based on the combination of voltage model and current model. It inherits the merits of both the voltage model and current model, i.e., high robustness to machine parameters in high speed range from and low sensitivity to disturbance voltages in low speed range. The state equation of the stator flux can be given by (15). The equation is written using α-β complex vector notation where $\boldsymbol{f}_{\alpha\beta}=f_\alpha+jf_\beta$.

$$\frac{d\boldsymbol{\psi}_{\alpha\beta}}{dt}=\boldsymbol{u}_{\alpha\beta}-R_s\boldsymbol{i}_{\alpha\beta}+\Delta\boldsymbol{u}_{\alpha\beta} \tag{15}$$

where $\boldsymbol{\psi}_{\alpha\beta}$, $\boldsymbol{u}_{\alpha\beta}$, $\Delta\boldsymbol{u}_{\alpha\beta}$ and $\boldsymbol{i}_{\alpha\beta}$ are the stator flux linkages, armature voltages, disturbance voltages and the armature currents in the α-β reference frame.

The stator flux observer constructed for system expressed by (15) can be written in the form of

$$\begin{cases}\tilde{\boldsymbol{\psi}}_{\alpha\beta}=\hat{\boldsymbol{\psi}}_{\alpha\beta}-\boldsymbol{\psi}_{\alpha\beta i}\\ \dfrac{d\hat{\boldsymbol{\psi}}_{\alpha\beta}}{dt}=\boldsymbol{u}_{\alpha\beta}-R_s\boldsymbol{i}_{\alpha\beta}+\Delta\hat{\boldsymbol{u}}_{\alpha\beta}-k_{po}\tilde{\boldsymbol{\psi}}_{\alpha\beta}\\ \dfrac{d\Delta\hat{\boldsymbol{u}}_{\alpha\beta}}{dt}=-k_{io}\tilde{\boldsymbol{\psi}}_{\alpha\beta}\end{cases} \tag{16}$$

where $\tilde{\boldsymbol{\psi}}_{\alpha\beta}$ and $\hat{\boldsymbol{\psi}}_{\alpha\beta}$ are the observation error and the estimated stator flux respectively, $\boldsymbol{\psi}_{\alpha\beta i}$ is the stator flux linkage obtained from current model, $\Delta\hat{\boldsymbol{u}}_{\alpha\beta}$ is the estimated value of $\Delta\boldsymbol{u}_{\alpha\beta}$, k_{po} and k_{io} are the observer gains.

The estimated stator flux-linkage can be obtained as

$$\hat{\boldsymbol{\psi}}_{\alpha\beta}=\frac{k_{po}s+k_{io}}{s^2+k_{po}s+k_{io}}\boldsymbol{\psi}_{\alpha\beta i}+\frac{s^2}{s^2+k_{po}s+k_{io}}\boldsymbol{\psi}_{\alpha\beta v} \tag{17}$$

where $\boldsymbol{\psi}_{\alpha\beta v}=\int\left(\boldsymbol{u}_{\alpha\beta}-R_s\boldsymbol{i}_{\alpha\beta}\right)dt$

It shows that the estimated stator flux is a combination of the current model stator flux filtered by a low pass filter and the voltage model stator flux filtered by a high pass filter. The gains k_{po} and k_{io} can be easily set by pole placement, i.e., $k_{po}=2\omega_o$, $k_{io}=\omega_o^2$, where ω_o is the undamped natural frequency and is usually set between 10Hz to 20Hz to make a smooth transition between the two models [18]. The block diagram of the flux observer in discrete time domain is shown in Fig. 5. The solid magenta line indicates the predicted stator flux. Since currents in the α-β reference frame are sinusoidal, the trapezoidal rule is used for approximating the integral, hence the estimated current $\boldsymbol{i}_{\alpha\beta}(k+1|k)$ is employed in the stator flux observer.

In this paper, the DB-DTFC in the *d*–*q* reference frame and in the *M*-*T* reference frame are briefed as DB-DTFC-DQ and

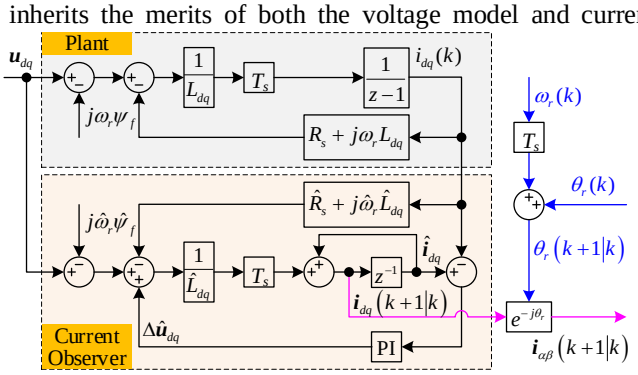

Fig. 4. Block diagram of the digital current observer.

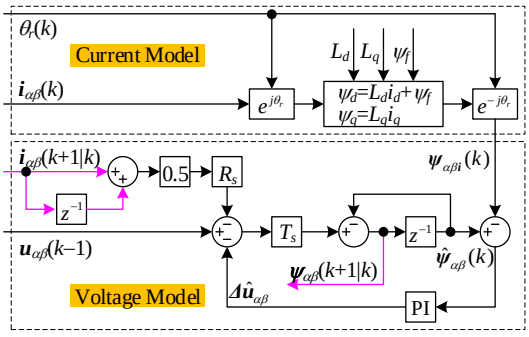

Fig. 5. Block diagram of the digital stator flux observer.

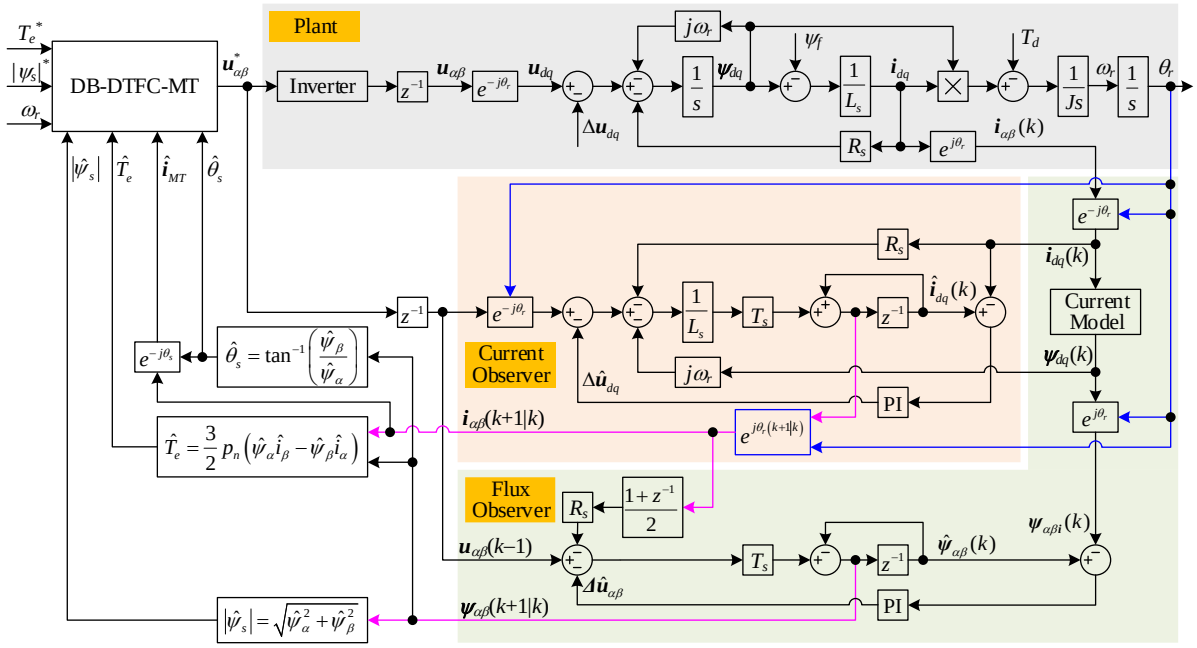

Fig. 6. The block diagram of the entire DB-DTFC-MT system.

DB-DTFC-MT, respectively. The block diagram of the entire DB-DTFC-MT system is shown in Fig. 6. The overall block diagram of the speed regulation system is shown in Fig. 7.

IV. Robustness to Parameter Variations

As shown in Fig. 7, a simple maximum torque per ampere (MTPA) control strategy without flux-weakening is employed in the control system since the aim of this paper is the solve the one-step delay problem. There are three modules in the control system are affected by the motor parameters, namely the stator flux and current observer module, the MTPA module, and the DB-DTFC-MT controller module.

The stator flux observer and the current observer have been widely studied by many researchers since they are the key parts in the high-performance CVC or DTFC [8], [9], [18], [21], [24]. In [8], the stator current observer is proved to be insensitive to parameters variation below the crossover frequency. In [9], it is verified that the stator flux observer appears to be sensitive to the parameter variations below its crossover frequency but becomes more robust to parameter variations as speed increases. In order to improve the robustness of the MTPA

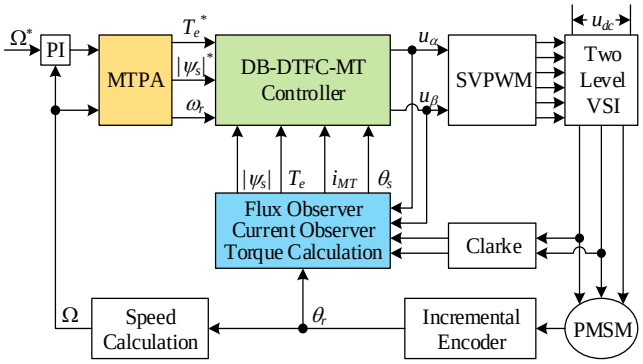

Fig. 7. Block diagram of the speed regulation system.

method, the MTPA strategies that insensitive to parameter variations are studied by S. Morimoto group [25]-[27]. In the DB-DTFC-DQ system, it is difficult to have a theoretical analysis of the robustness due to the nonlinear and cross-coupling relationship between the state variables and the manipulated inputs. However, in the DB-DTFC-MT system, the relationship between the state variables and the manipulated inputs is linearized, hence a theoretical analysis of the controller becomes possible. In this paper, the discussion of the robustness is focused on the DB-DTFC-MT controller module with assumption that the stator observer module and the MTPA module are insensitive to parameter variations.

Suppose the parameters used in the controller is mismatched, then the state equations of the stator flux and torque can be expressed as

$$\begin{cases} \dfrac{d|\psi_s|}{dt} = u_M - \hat{R}_s i_M = u_M - R_s i_M - \Delta u_M \\ \dfrac{dT_e}{dt} = \hat{A}(u_T - R_s i_T - \omega_r |\psi_s| - \Delta u_T) \end{cases} \tag{18}$$

where

$$\Delta u_M = (\hat{R}_s - R_s) i_M = \tilde{R}_s i_M$$

$$\Delta u_T = (\hat{R}_s - R_s) i_T + (\hat{\omega}_s - \omega_s)|\psi_s| = \tilde{R}_s i_T + \tilde{\omega}_s |\psi_s|$$

$$\hat{A} = \frac{3 p_n}{2 \hat{L}_d \hat{L}_q}\left[\hat{L}_q \hat{\psi}_f \cos\delta + \left(\hat{L}_d - \hat{L}_q\right)|\psi_s| \cos 2\delta\right]$$

It shows that the mismatched resistance leads to the disturbance voltages, while the mismatched permanent magnet flux, *d*- and *q*-axis inductances lead to the mismatched torque control gain. These disturbance voltages and mismatched control gain have some effect on the system control performance.

A. The Effect of the Disturbance Voltages

From Fig. 3, it can be known that the deadbeat controller is a compound controller consisting of the proportional feedback control law and the disturbance feedforward compensation. Nevertheless, the deadbeat controller is a nonlinear controller because the proportional gain $1/T_s$ is so high that the manipulated output is saturated in most of the dynamic process. In the last few steps of the tracking process, the deadbeat controller is linear because the tracking error is very small. Therefore, the steady-state tracking error can be calculated as that in a linear controller. Consequently, the steady-state tracking error of the stator flux and torque can be expressed as

$$\begin{cases} \Delta|\psi_s| = \Delta u_M T_s \\ \Delta T_e = A\Delta u_T T_s \end{cases} \tag{19}$$

Since T_s is very small, the steady-state tracking error is small also, which means the system has good robustness to the resistance variations.

B. The Effect of the Mismatched Torque Control Gain

As proved in [28], though the control gain causes no steady-state tracking error for the constant reference, it has a significant impact on the dynamic performance of the control system. If the control gain is smaller than the nominal value, the feedforward gain of the torque control system is overestimated, thus the tracking performance the disturbance rejection property can be improved, whereas the noise suppression performance is deteriorated and vice versa. It should be noted that the deadbeat controller is very sensitive to the measurement noise, which means the torque response is prone to be oscillating if the control gain is underestimated.

The torque control gain A has a complicated relationship with the permanent magnet flux. Since the torque angle δ is generally small, it can be set to zero in the control system, then the torque control gain can be simplified as

$$\hat{A} = \frac{3p_n}{2}\left(\frac{|\psi_s|}{\hat{L}_q} - \frac{|\psi_s| - \hat{\psi}_f}{\hat{L}_d}\right) \tag{20}$$

For the PMSM used in this paper, the permanent magnet flux dominates the stator flux, thus the control gain is sensitive to the permanent magnet flux. On the other hand, the difference between the stator flux and the permanent magnet flux is small when the permanent magnet flux equals its nominal value, hence the control gain is insensitive to the d- and q-axis inductances. However, the situation will be different when the permanent magnet flux is mismatched, specific analysis is not addressed here.

V. Experimental Results

A. Test Bench Setup

Table I lists the parameters of the PMSM used in this paper. The DB-DTFC-MT scheme is implemented in the inverter with the same PWM switching frequency and the sampling frequency, i.e., 10kHz. The DS1103 dSPACE real-time control platform with TMS320F2407 as the core processor is built to test the proposed designs experimentally. The phase currents and the DC bus voltage are measured by the hall effect current sensor CSM100B and the hall effect voltage sensor VSM025A made by Chahua-Electric Co., Ltd. After obtaining the voltage and current, the stator flux is observed first by the closed-loop observer, then the torque can be calculated by the stator flux and current. The schematic diagram and the configuration of the test bench are shown in Fig. 8 and Fig. 9, respectively.

The DC bus voltage u_{dc} is set to 150V and the saturation limit of the phase current is 6 A. A PI controller is used to regulate the speed with an undamped natural frequency of 60 rad/s. The bandwidth of the flux observer and the current observer is set to 20Hz and 300Hz, respectively.

TABLE I
MACHINE PARAMETERS OF EXAMINED PMSM.

Symbol	Quantity	Symbol	Quantity
Rated power P_N	1.5 (kW)	Stator resistance R	0.9 (Ω)
Rated voltage U_N	220 (V)	D axis inductance L_d	2.0 (mH)
Rated speed n_N	7500 (rpm)	Q axis inductance L_q	3.7 (mH)
Rated torque T_N	2.2 (N·m)	Permanent flux ψ_f	0.0915 (Wb)
Phase current Limit I_{smax}	6 (A)	Motor inertia J	2.38×10^{-4} (kg·m^2)
Number of pole-pairs p_n	2	Friction torque T_f	0.1 (N·m)

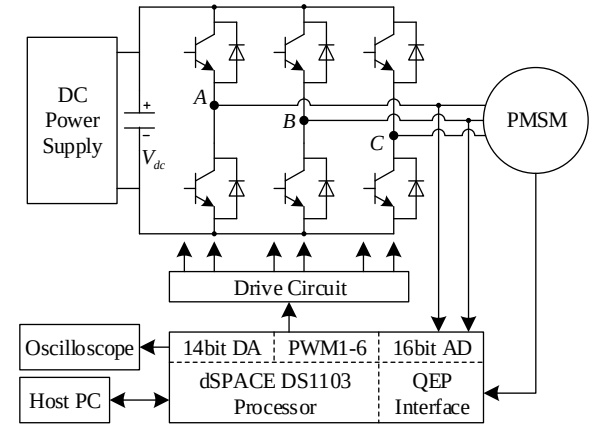

Fig. 8. The schematic diagram of test bench.

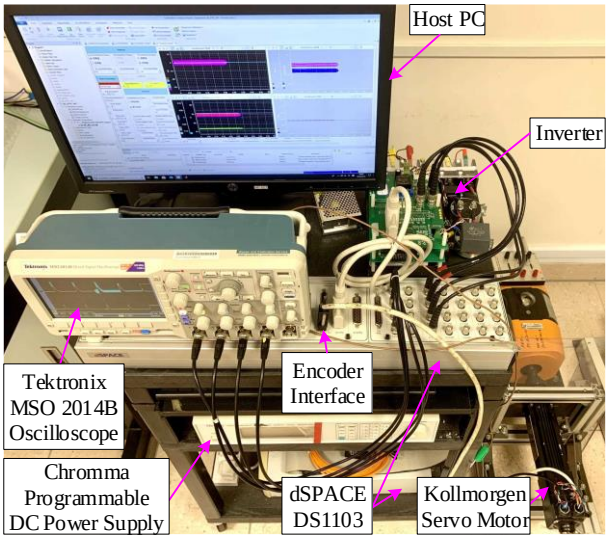

Fig. 9. Configuration of the test bench.

B. Experimental Verification

To evaluate the dynamic performance of the DB-DTFC-MT scheme under different speeds, the speed reference is stepped from 0 rpm to 5000 rpm in steps of 1000 rpm. The DB-DTFC-MT scheme is tested in three cases.

In case 1, the stator flux is observed by the stator flux observer without prediction, and the measured current is used for the calculation. The experimental results are shown in Fig. 10. The zoom views from 0 ms to 3 ms and from 599 ms to 603 ms are shown in Fig. 10(b). It shows that the torque and the stator flux are oscillating. The oscillation is more intense in the low-speed range because of the faster dynamic response.

In case 2, the stator flux is predicted by the stator flux observer, while the stator current used here is still the measured one. The experimental results are shown in Fig. 11. Compared with case 1, a great reduction of the oscillation can be found in the stator flux, while not in the torque.

In case 3, both the stator flux and current are predicted by their observers. The experimental results are shown in Fig. 12. It can be seen that deadbeat control is realized in both the torque and the stator flux, without oscillation and steady-state tracking error. Due to the voltage limitation, the torque takes more time to reach its reference value at higher speeds. It should be noted that the predicted torque and stator flux are smooth because the low bandwidth stator flux observer plays a good role in suppressing the measurement noise. Nevertheless, the current i_d and i_q shows that the actual torque and stator flux are well controlled.

As a comparison, the same flux and current prediction method are used in the DB-DTFC-DQ system, and the experimental results are shown in Fig. 13. Similarly, the oscillation is eliminated by predicting the stator flux and the current. However, due to the cross-coupling relationship, the torque and the stator flux take the same time to reach their references. When the voltage is saturated, the voltage vectors selection strategy must be changed to avoid losing control of the torque and stator flux simultaneously.

In the torque control loop, the tracking performance is one of the most important control performances and it should be verified in various operating conditions. Therefore, some typical test signals, such as sinusoidal signals, step signals, and trapezoidal signals are used for the verification, as shown in Fig. 14. In Fig. 14(a), the speed reference is a sinusoidal signal with an amplitude of 4000 rpm and a frequency of 2Hz. Due to the low frequency, the torque reference is also sinusoidal since it is not saturated. The distortion in the torque reference is caused by the nonlinear friction torque. When the frequency of the sinusoidal speed reference is increased to 10Hz, the torque reference is trapezoidal due to the saturation, as shown in Fig. 14(b). In Fig. 14(c), the speed reference is a step signal with steps of 2500 rpm, thus the torque reference is also a step signal.

In Fig. 14(a) and (b), the torque is well tracked while a small tracking error exists in the stator flux response. The stator flux tracking error is caused stator flux observer. A PI regulator is used in the stator flux observer, thus the observation error can be eliminated only when observing a constant stator flux, as shown in Fig. 14(c). For the sinusoidal stator flux, the observation error will be produced, and it increases with the frequency. Though the stator flux tracking error is very small, it leads to a big variation in the *d*-axis current because of the small *d*-axis inductance. As will be proved in the next section, the

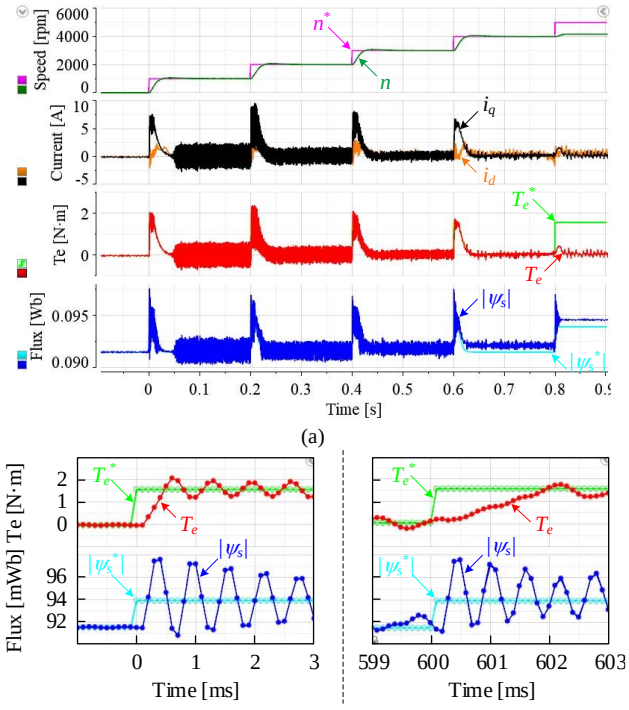

Fig. 10. Transient response of DB-DTFC-MT in case 1. (a) Overall view (b) Zoom view from 0 ms to 3 ms and from 599 ms to 603 ms.

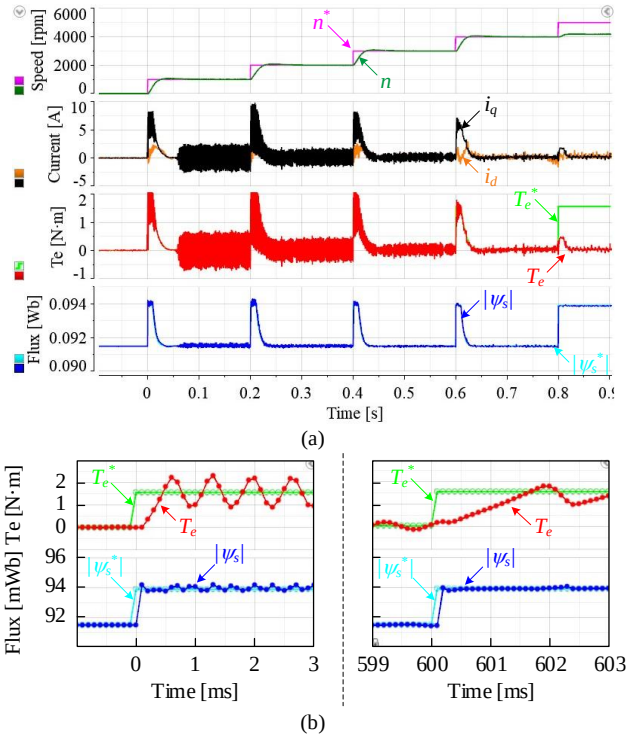

Fig. 11. Transient response of DB-DTFC-MT in case 2. (a) Overall view. (b) Zoom view from 0 ms to 3 ms and from 599 ms to 603 ms.

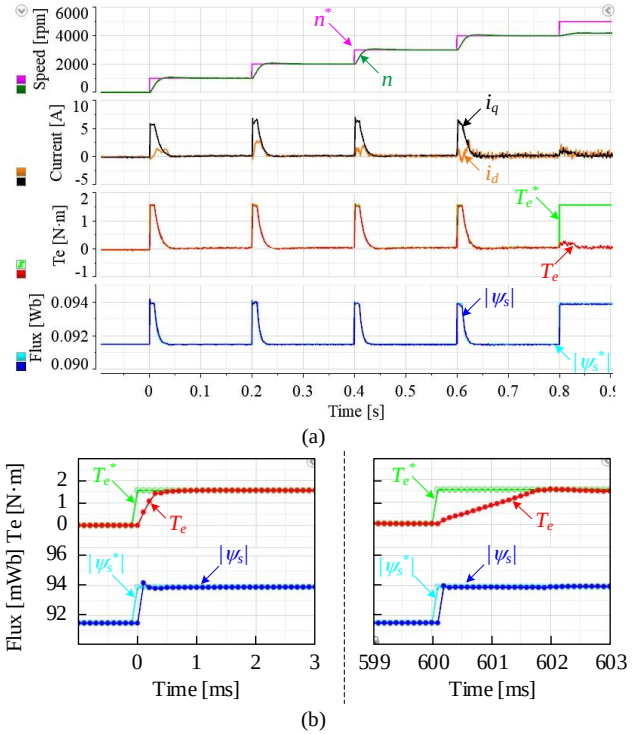

Fig. 12. Transient response of DB-DTFC-MT in case 3. (a) Overall view. (b) Zoom view from 0 ms to 3 ms and from 599 ms to 603 ms.

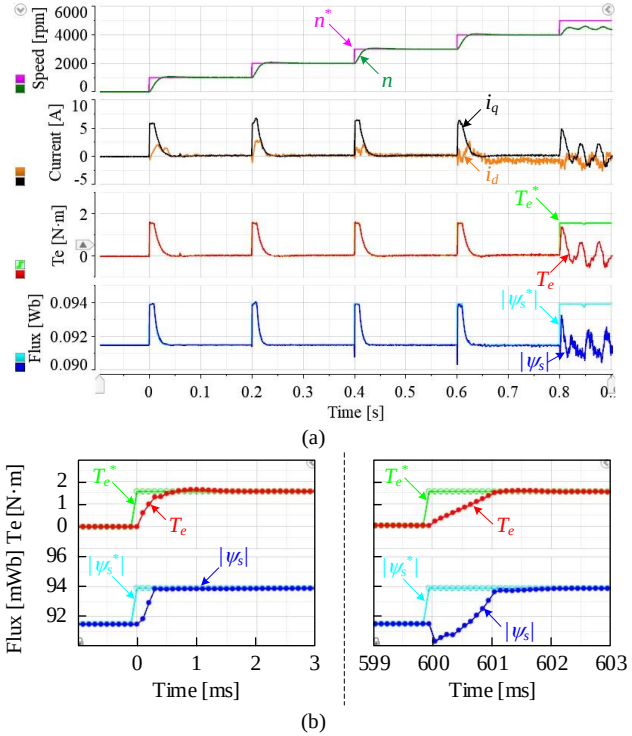

Fig. 13. Transient response of DB-DTFC-DQ. (a) Overall view. (b) Zoom view from 0 ms to 3 ms and from 599 ms to 603 ms.

d-axis inductance has a little impact on the system dynamic performance. Therefore, a larger *d*-axis inductance can be used for reducing the pulsation in the *d*-axis current.

These experimental results show that the proposed DB-DTFC-MT scheme can be applied in various operating situations with good tracking performance.

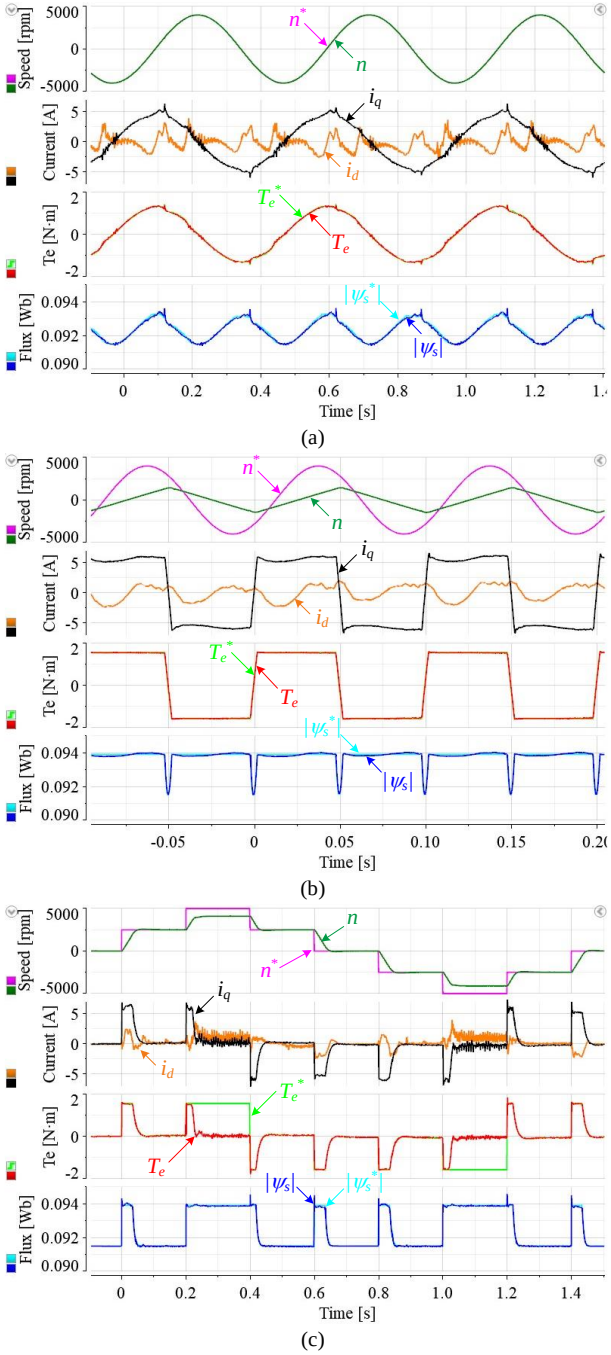

Fig. 14. Experimental results under different sinusoidal speed references. (a) n_{ref}=4000sin(4π*t*). (b) n_{ref}=4000sin(20π*t*). (c) Wide speed reversal.

C. Parameter Sensitivity

In order to evaluate the sensitivity of the control system to parameter variations, the control system operating with mismatched parameters is tested. Firstly, the effect of the disturbance voltages caused by the mismatched stator resistance is tested. When the stator resistance is decreased by 100% and increased by 300%, the experimental results are shown in Fig. 15 and Fig. 16, respectively. It shows that the mismatched stator resistance leads to the steady-stated tracking error in both torque

and stator flux, which is consistent with the theory.

Secondly, the effect of the control gain is tested. When the permanent magnet flux is mismatched by 30%, the experimental results are shown in Fig. 17 and Fig. 18. As shown in Fig. 17, when the estimated permanent magnet flux is decreased by 30%, the torque response is oscillating, especially at the low-speed range. In contrast, when the estimated permanent magnet flux is increased by 30%, the torque response is slow down whereas the stability of the system is improved.

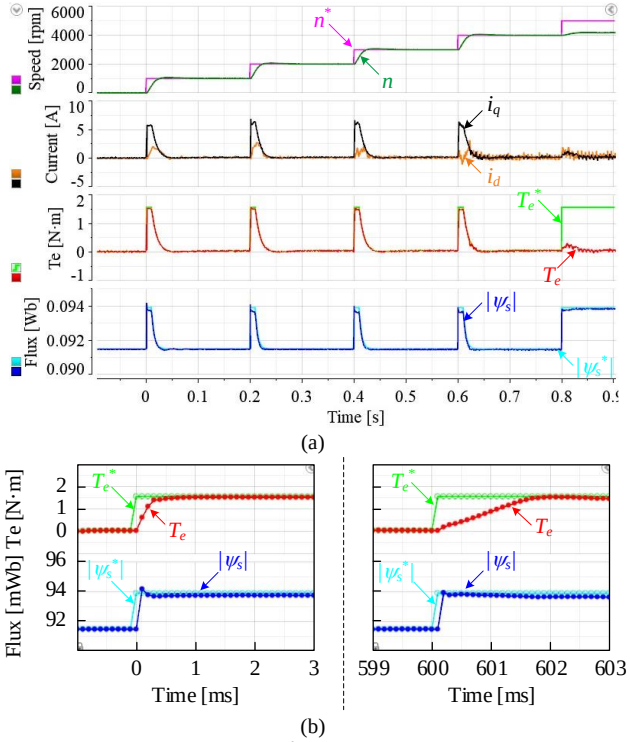

Fig. 15. Transient response when $\hat{R}_s = 0$. (a) Overall view. (b) Zoom view from 0 ms to 3 ms and from 599 ms to 603 ms.

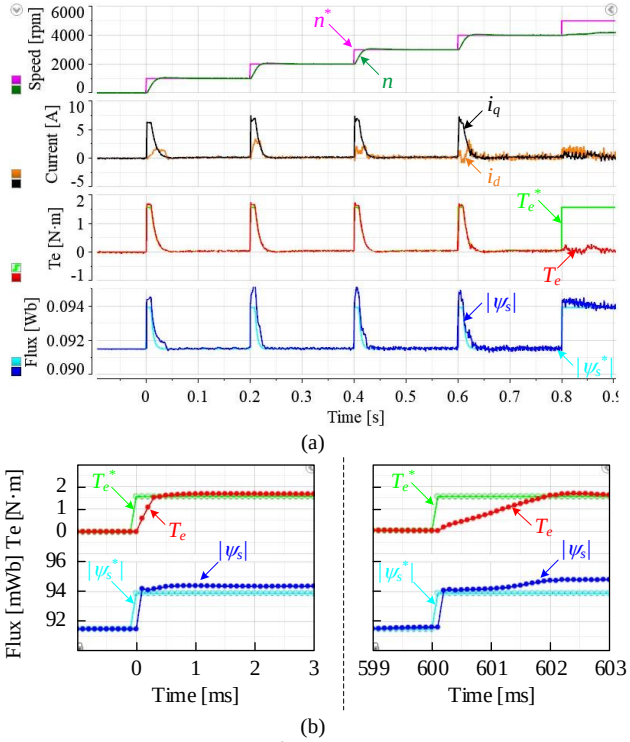

Fig. 16. Transient response when $\hat{R}_s = 4R_s$. (a) Overall view. (b) Zoom view from 0 ms to 3 ms and from 599 ms to 603 ms.

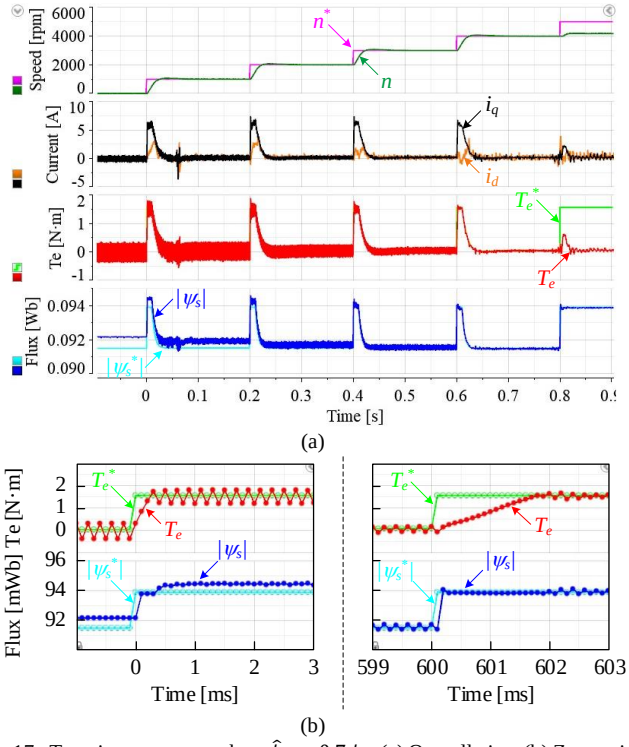

Fig. 17. Transient response when $\hat{\psi}_f = 0.7\psi_f$. (a) Overall view (b) Zoom view from 0 ms to 3 ms and from 599 ms to 603 ms.

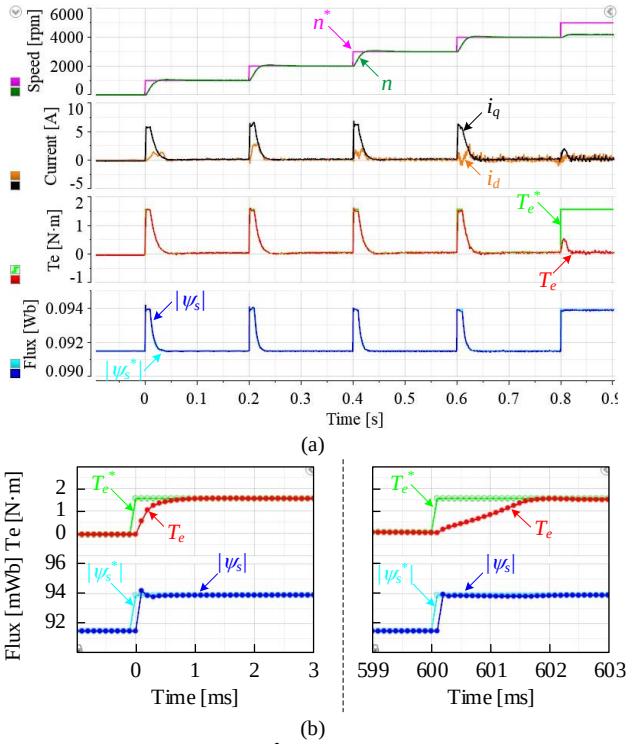

Fig. 18. Transient response when $\hat{\psi}_f = 1.3\psi_f$. (a) Overall view (b) Zoom view from 0 ms to 3 ms and from 599 ms to 603 ms.

When the q-axis inductance is mismatched by 40%, the experimental results are shown in Fig. 19 and Fig. 20. When the estimated q-axis inductance is increased by 40%, the control gain is decreased, resulting in faster dynamic response. Vice versa. It is found in the experiments that oscillation will be produced when the estimated q-axis inductance is increased by 50% and more.

As analyzed earlier, the control gain is quite insensitive to the d-axis inductance, hence larger variations in the estimated d-axis inductance is tested. The experimental results when the estimated d-axis inductance is decreased by 90% and increased by 400% are shown in Fig. 21 and Fig. 22, respectively. In Fig.

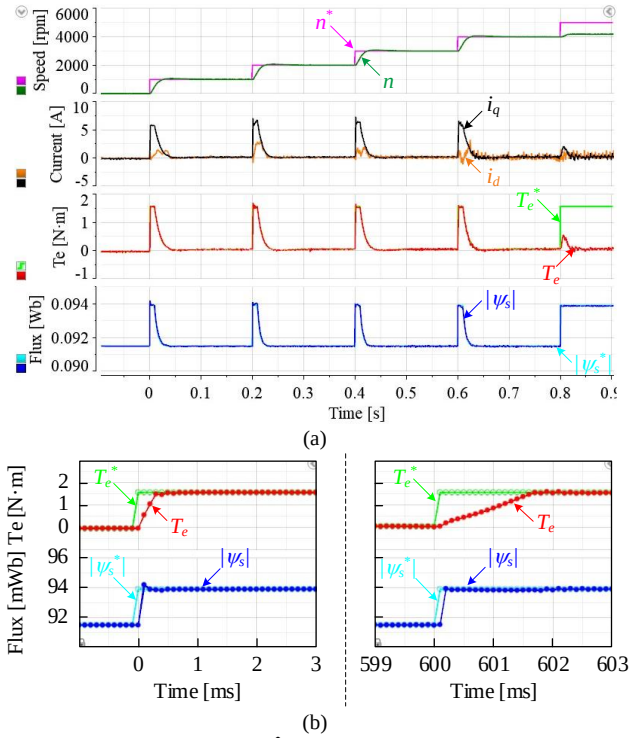

Fig. 19. Transient response when $\hat{L}_q = 1.4L_q$. (a) Overall view (b) Zoom view from 0 ms to 3 ms and from 599 ms to 603 ms.

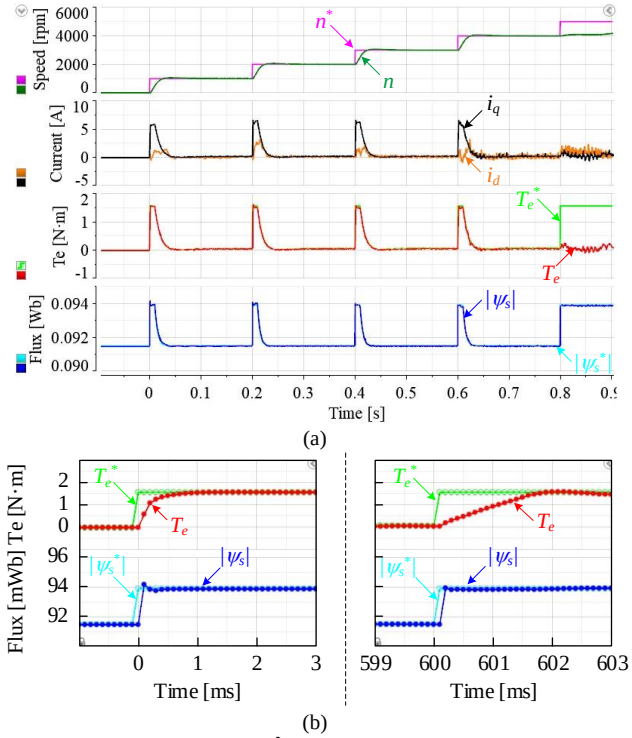

Fig. 20. Transient response when $\hat{L}_q = 0.6L_q$. (a) Overall view (b) Zoom view from 0 ms to 3 ms and from 599 ms to 603 ms.

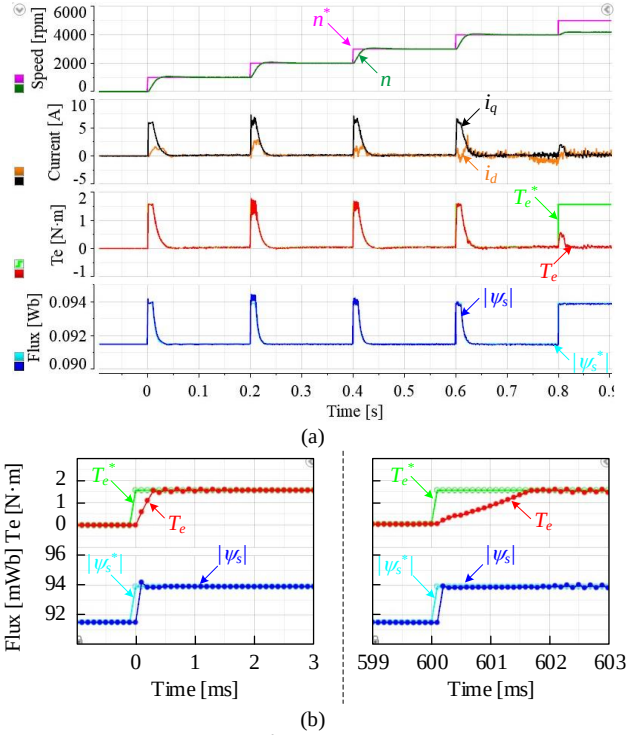

Fig. 21. Transient response when $\hat{L}_d = 0.1L_d$. (a) Overall view. (b) Zoom view from 0 ms to 3 ms and from 599 ms to 603 ms.

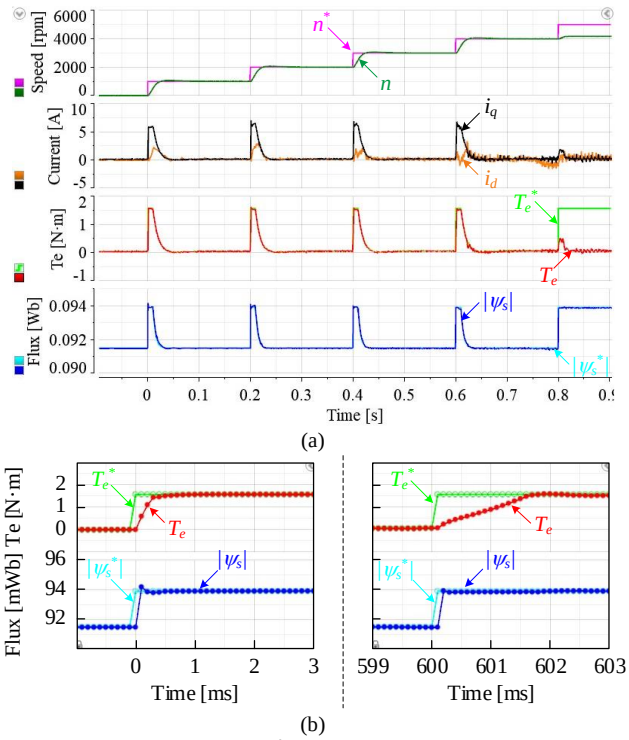

Fig. 22. Transient response when $\hat{L}_d = 5L_d$. (a) Overall view. (b) Zoom view from 0 ms to 3 ms and from 599 ms to 603 ms.

TABLE II
PARAMETER VARIATION RANGES FOR STABLE OPERATION.

Parameters	Variation ranges for stable operation
R_s	-100% ~ +300%
ψ_f	-10% ~ +30%
L_q	-60% ~ +40%
L_d	-80% ~ +400%

21, it can be found that the system tends to oscillate in the high-current region where the stator flux magnitude is larger than the one in the low-current region. In Fig. 22, it can be seen that the system dynamic performance is hardly affected even the estimated *d*-axis inductance has been five times of its nominal value.

According to the above analysis, it can be concluded that the proposed DB-DTFC-MT controller shows some sensitivity to the permanent magnet flux whereas has strong robustness to the stator resistance and the inductances, especially the *d*-axis inductance. In order to show the robustness of the system to parameter variations intuitively, the parameter variation ranges that can make the system run stably are shown in Table II.

VI. Conclusion

In this paper, the digital implementation of DB-DTFC in the *M-T* reference frame is derived. Due to the one-step delay of the digital system, the stator flux and torque will oscillate seriously in low-speed range if the stator flux and stator current are not predicted. In order to achieve real deadbeat control, the stator flux and stator current in the next sampling instant are predicted by the proposed digital flux observer and current observer. The proposed DB-DTFC-MT controller is verified to have a good tracking performance in various operating conditions. Due to the linearization of the state equations in the *M-T* reference frame, the theoretical analysis the effect of the motor parameter variations becomes possible. Though the proposed DB-DTFC-MT controller shows some sensitivity to the permanent magnet flux, it has strong robustness to the stator resistance and the inductances, especially the *d*-axis inductance. Since the *d*-axis inductance has little impact on the system dynamic performance, a larger *d*-axis inductance can be used for reducing the pulsation in the *d*-axis current when tracking a sinusoidal torque reference. The effectiveness of the method is verified by experiments conducted on a platform based on dSPACE DS1103.

References

[1] R. D. Lorenz, "The emerging role of dead-beat, direct torque and flux control in the future of induction machine drives," *2008 11th International Conference on Optimization of Electrical and Electronic Equipment*, Brasov, 2008, p. XIX-XXVII.

[2] Y. Wang, Y. Shi, Y. Xu, and R. D. Lorenz, "A comparative overview of indirect field oriented control (IFOC) and deadbeat-direct torque and flux control (DB-DTFC) for AC Motor Drives," *Chin. J. Electr. Eng.*, vol. 1, no. 1, pp. 9-20, Dec. 2015.

[3] X. Zhu, C. H. T. Lee, C. C. Chan, L. Xu, and W. Zhao, "Overview of flux-modulation machines based on flux-modulation principle: Topology, theory and development prospects," *IEEE Trans. Transp. Electrific.*, vol. 6, no. 2, pp. 612-624, Jun. 2020.

[4] S. Saponara, C. H. T. Lee, N. X. Wang, and J. L. Kirtley, "Electric drives and power chargers: recent solutions to improve performance and energy efficiency for hybrid and fully electric vehicles," *IEEE Veh. Technol. Mag.*, vol. 15, no. 1, pp. 73-83, Mar. 2020.

[5] T. G. Habetler, F. Profumo, M. Pastorelli, and L. M. Tolbert, "Direct torque control of induction machines using space vector modulation," *IEEE Trans. on Ind. Applicat.*, vol. 28, no. 5, pp. 1045-1053, Sep/Oct. 1992.

[6] G. S. Buja and M. P. Kazmierkowski, "Direct Torque Control of PWM Inverter-Fed AC Motors—A Survey," *IEEE Trans. Ind. Electron.*, vol. 51, no. 4, pp. 744-757, Aug. 2004.

[7] B. H. Kenny and R. D. Lorenz, "Stator- and rotor-flux-based deadbeat direct torque control of induction machines," *IEEE Trans. on Ind. Applicat.*, vol. 39, no. 4, pp. 1093-1101, Jul/Aug. 2003.

[8] J. S. Lee, C. Choi, J. Seok, and R. D. Lorenz, "Deadbeat-Direct Torque and Flux Control of Interior Permanent Magnet Synchronous Machines With Discrete Time Stator Current and Stator Flux Linkage Observer," *IEEE Trans. on Ind. Applicat.*, vol. 47, no. 4, pp. 1749-1758, Jul/Aug. 2011.

[9] J. S. Lee and R. D. Lorenz, "Robustness Analysis of Deadbeat-Direct Torque and Flux Control for IPMSM Drives," *IEEE Trans. Ind. Electron.*, vol. 63, no. 5, pp. 2775-2784, May. 2016.

[10] Y. Xu, C. Morito and R. D. Lorenz, "Extending High-Speed Operating Range of Induction Machine Drives Using Deadbeat-Direct Torque and Flux Control With Precise Flux Weakening," *IEEE Trans. on Ind. Applicat.*, vol. 55, no. 4, pp. 3770-3780, Jul/Aug. 2019.

[11] L. Zhong, M. F. Rahman, W. Y. Hu, and K. W. Lim, "Analysis of direct torque control in permanent magnet synchronous motor drives," *IEEE Trans. Power Electron.*, vol. 12, no. 3, pp. 528-536, May. 1997.

[12] G. Foo and M. F. Rahman, "Sensorless Direct Torque and Flux-Controlled IPM Synchronous Motor Drive at Very Low Speed Without Signal Injection," *IEEE Trans. Ind. Electron.*, vol. 57, no. 1, pp. 395-403, Jan. 2010.

[13] X. Zhang, G. H. B. Foo and M. F. Rahman, "A Robust Field-Weakening Approach for Direct Torque and Flux Controlled Reluctance Synchronous Motors With Extended Constant Power Speed Region," *IEEE Trans. Ind. Electron.*, vol. 67, no. 3, pp. 1813-1823, Mar. 2020.

[14] M. H. Vafaie, B. M. Dehkordi, P. Moallem, and A. Kiyoumarsi, "Improving the Steady-State and Transient-State Performances of PMSM Through an Advanced Deadbeat Direct Torque and Flux Control System," *IEEE Trans. Power Electron.*, vol. 32, no. 4, pp. 2964-2975, Apr. 2017.

[15] X. Lin, W. Huang, W. Jiang, Y. Zhao, and S. Zhu, "Deadbeat Direct Torque and Flux Control for Permanent Magnet Synchronous Motor Based on Stator Flux Oriented," *IEEE Trans. Power Electron.*, vol. 35, no. 5, pp. 5078-5092, May. 2020.

[16] I. Boldea, M. C. Paicu and G. D. Andreescu, "Active Flux Concept for Motion-Sensorless Unified AC Drives," *IEEE Trans. Power Electron.*, vol. 23, no. 5, pp. 2612-2618, Sep. 2008.

[17] G. Andreescu, C. I. Pitic, F. Blaabjerg, and I. Boldea, "Combined Flux Observer With Signal Injection Enhancement for Wide Speed Range Sensorless Direct Torque Control of IPMSM Drives," *IEEE Trans. Energy Convers.*, vol. 23, no. 2, pp. 393-402, Jun. 2008.

[18] P. L. Jansen and R. D. Lorenz, "A physically insightful approach to the design and accuracy assessment of flux observers for field oriented induction machine drives," *IEEE Trans. on Ind. Applicat.*, vol. 30, no. 1, pp. 101-110, Jan/Feb. 1994.

[19] A. Aliaskari, B. Zarei, S. A. Davari, F. Wang, and R. M. Kennel, "A Modified Closed-Loop Voltage Model Observer Based on Adaptive Direct Flux Magnitude Estimation in Sensorless Predictive Direct Voltage Control of an Induction Motor," *IEEE Trans. Power Electron.*, vol. 35, no. 1, pp. 630-639, Jan. 2020.

[20] X. Lin, W. Huang, W. Jiang, Y. Zhao, and S. Zhu, "A Stator Flux Observer With Phase Self-Tuning for Direct Torque Control of Permanent Magnet Synchronous Motor," *IEEE Trans. Power Electron.*, vol. 35, no. 6, pp. 6140-6152, Jun. 2020.

[21] N. T. West and R. D. Lorenz, "Digital Implementation of Stator and Rotor Flux-Linkage Observers and a Stator-Current Observer for Deadbeat Direct Torque Control of Induction Machines," *IEEE Trans. on Ind. Applicat.*, vol. 45, no. 2, pp. 729-736, Mar/Apr. 2009.

[22] Y. Xu, C. Morito and R. D. Lorenz, "Accurate Discrete-Time Modeling for Improved Torque Control Accuracy for Induction Machine Drives at Very Low Sampling-to-Fundamental Frequency Ratios," *IEEE Trans. Transp. Electrific.*, vol. 6, no. 2, pp. 668-678, Jun. 2020.
[23] W. Xu and R. D. Lorenz, "High-Frequency Injection-Based Stator Flux Linkage and Torque Estimation for DB-DTFC Implementation on IPMSMs Considering Cross-Saturation Effects," *IEEE Trans. on Ind. Applicat.*, vol. 50, no. 6, pp. 3805-3815, Nov/Dec. 2014.
[24] A. Yoo and S. Sul, "Design of Flux Observer Robust to Interior Permanent-Magnet Synchronous Motor Flux Variation," *IEEE Trans. on Ind. Applicat.*, vol. 45, no. 5, pp. 1670-1677, Sep/Oct. 2009.
[25] T. Inoue, Y. Inoue, S. Morimoto, and M. Sanada, "Mathematical Model for MTPA Control of Permanent-Magnet Synchronous Motor in Stator Flux Linkage Synchronous Frame," *IEEE Trans. on Ind. Applicat.*, vol. 51, no. 5, pp. 3620-3628, Sept/Oct. 2015.
[26] A. Shinohara, Y. Inoue, S. Morimoto, and M. Sanada, "Direct Calculation Method of Reference Flux Linkage for Maximum Torque per Ampere Control in DTC-Based IPMSM Drives," *IEEE Trans. Power Electron.*, vol. 32, no. 3, pp. 2114-2122, Mar. 2017.
[27] A. Shinohara, Y. Inoue, S. Morimoto, and M. Sanada, "Maximum Torque Per Ampere Control in Stator Flux Linkage Synchronous Frame for DTC-Based PMSM Drives Without Using q-Axis Inductance," *IEEE Trans. on Ind. Applicat.*, vol. 53, no. 4, pp. 3663-3671, Jul/Aug. 2017.
[28] Y. Zuo, X. Zhu, L. Quan, C. Zhan, Y. Du, and Z. Xiang, "Active Disturbance Rejection Controller for Speed Control of Electrical Drives Using Phase-Locking Loop Observer," *IEEE Trans. Ind. Electron.*, vol. 66, no. 3, pp. 1748-1759, Mar. 2019.
[29] Y. Zuo, J. Mei, X. Zhang, and C. H. T. Lee, "Simultaneous Identification of Multiple Mechanical Parameters in a Servo Drive System Using Only One Speed," *IEEE Trans. Power Electron.*, vol. 36, no. 1, pp. 716-726, Jan. 2021.

Yuefei Zuo (M'18) received the B.Sc. and the Ph. D. degrees in electrical engineering and automation from Nanjing University of Aeronautics and Astronautics, Nanjing, China, in 2010 and 2016, respectively.

He has been working as a Lecturer at Jiangsu University since July 2016. He is currently a Postdoctoral Research Fellow with the School of Electrical and Electronic Engineering, Nanyang Technological University, Singapore. His research interests include advanced control strategies for high performance electric drives.

Jie Mei (S'13) received his B.S. degree in electrical engineering from the School of Electrical and Computer Engineering, Georgia Institute of Technology, Atlanta, GA, USA, in 2015. He is currently pursuing his Ph.D. degree at the Department of Electrical Engineering and Computer Science, Massachusetts Institute of Technology, Cambridge, MA, USA. His research interests include Electric Machines, Multi-Carrier Energy System, and Electric Vehicle Technologies.

Chaoqiang Jiang (S'16, M'19) received the B.Eng. and M.Sc. degrees in electrical engineering and automation from Wuhan University, Wuhan, China, in 2012 and 2015, respectively, and the Ph.D. degree in electrical and electronic engineering from The University of Hong Kong, Hong Kong, in 2019.

He is currently a Postdoctoral Research Associate at the University of Cambridge, U.K. In 2019, he was a Visiting Researcher at the Nanyang Technological University, Singapore. His current research interests include power electronics, wireless power transfer techniques, electric machines and drives, and electric vehicle (EV) technologies.

Christopher H. T. Lee (M'12-SM'18) received his B.Eng. (First Class Honours) degree, and Ph.D. degree both in electrical engineering from Department of Electrical and Electronic Engineering, The University of Hong Kong, Hong Kong, in 2009 and 2016, respectively.

He currently serves as an Assistant Professor at Nanyang Technological University, Singapore, a Visiting Assistant Professor at Massachusetts Institute of Technology, United States, and also a Honorary Assistant Professor at The University of Hong Kong, Hong Kong. He is an Associate Editor for IEEE Access and IET Renewable Power Generation. His research interests include Electric Machines and Drives, Renewable Energies, and Electromechanical Propulsion Technologies. In these areas, he has published 1 book, 3 books chapters, and over 80 referred papers.

Dr. Lee has received many awards, including NRF Fellowship, Nanyang Assistant Professorship, Li Ka Shing Prize (the best Ph.D. thesis prize) and Croucher Foundation Fellowship.